Monolayer Solid ^{4}He Clusters on Graphite

M. E. Pierce and E. Manousakis
Department of Physics and Center for Materials Research and Technology, Florida State University, Tallahassee, FL 32306-4350

(February 1, 2008)

In order to resolve the controversy about the low density region of the phase diagram of the ^{4}He monolayer on graphite, we have undertaken a path integral Monte Carlo study of the system. We provide direct evidence that the low density monolayer possesses solid clusters and a low density vapor as opposed to the most recent proposal that the system is in a superfluid phase. We further establish that the rounded heat capacity peaks observed at low densities are caused by melting of such solid clusters and are not associated with the suggested superfluid transition.

PACS numbers 67.70.+n, 67.40 Kh

Monolayer helium adsorbed on graphite has long proven to be a fascinating system for studying the growth and behavior of a quantum film above an atomically ordered, uniform substrate and has been used to investigate a number of nearly two-dimensional (2D) phenomena [1–3]. A very prominent feature of this layer is a commensurate solid phase in which one-third of the available substrate adsorption sites are occupied [4–7]. For densities above the commensurate, the system is known to pass through a region of domain wall phases before forming an incommensurate triangular solid phase. On the other hand, the nature of the phase diagram below the commensurate density at low temperatures is less well established, with two competing pictures. One possibility is that the phase is a solid with vacancies [8]. At low temperatures, the vacancies coalesce, producing coexistence between a solid cluster and a vapor. More recently, it has been suggested that the solid melts if the density is decreased, and there is a low temperature liquid phase [9]. The first layer would then be a candidate in the search for a monolayer superfluid [9,10].

The solid cluster picture has been discussed by Ecke *et al* [8]. They note that since the commensurate solid phase is in the same universality class as the three-state Potts model [11–13], then at lower densities the film should consist of a commensurate solid with vacancies. If the temperature is raised, the solid melts continuously. Lowering the temperature causes the vacancies to coalesce (phase separate), a first order transition. The difference between the temperatures of these two transitions becomes smaller as the density is lowered until they meet at a tricritical point. This point was determined [8] to be at about 0.039 atom/$\mathring{A}^2$ and 1.3 K. Thus, in this picture, the monolayer consists of solid clusters surrounded by a low density vapor at low temperatures and densities.

More recent experiments have questioned this conclusion. Greywall and Busch [9] point out that the heat capacity is not linear in density for the entire region below the commensurate density, as it must be for solid-vapor coexistence [1]. They instead propose that the system has a self-bound liquid phase at about 0.04 atom/$\mathring{A}^2$. This conclusion is supported by 2D variational calculations for helium [14] that take substrate corrugations into account. The possibility of a first layer liquid is intriguing since at low temperatures it would be a superfluid above a bare substrate, with no underlying "dead" layer of helium. However, direct measurements [15] on the first layer detect no superfluidity. This negative result has been attributed to poor substrate connectivity.

In order to resolve this controversy, we have undertaken a path integral Monte Carlo (PIMC) study of the low density first layer. This is the first attempt to directly investigate this region by an exact, first principles method that treats the full quantum many-body problem. From our calculations, we provide the first direct evidence that the low density monolayer consists of solid clusters. No liquid phase occurs, and so there is no possibility for first layer superfluidity. We further establish that the rounded heat capacity peaks observed at low densities are caused by the melting of solid clusters and are not associated with a superfluid film, as has been suggested [9].

Our PIMC calculations use realistic helium-helium [16] and helium-substrate interactions. In order to include the effects of substrate corrugations, we use the full, anisotropic helium-graphite potential of Ref. [17]. For a general discussion of the PIMC method and its application to films, see Refs. [18,19]. In test runs, we determined that an inverse temperature slice of $\tau = 1/200K^{-1}$ was required to reach the desired accuracy using the semiclassical approximation for the required high temperature density matrix at 200 K. The semiclassical approximation allows substrate corrugations to be easily implemented. From the same test runs, we determined that an $l = 3$ multilevel bisection was required. All of our calculations are performed in a simulation cell with periodic boundary conditions and dimensions $25.560\mathring{A} \times 22.136\mathring{A}$ that exactly accommodates the commensurate solid The number of particles ranged from 20 to 40, with 36 corresponding to the commensurate density, $\rho_c = 0.0636$ atom/$\mathring{A}^2$. We also allowed for the possibility of particle permutations at low densities, but did not observe any.

It is essential that corrugations be included in the calculations because the commensurate solid phase is entirely the result of the substrate corrugations. A recent simulation for the helium monolayer [20] using the laterally averaged graphite potential [17] finds that the equilibrium phase is a liquid. Full solidification does not occur until the coverage is well above ρ_c. At ρ_c, the film on the featureless substrate is a compressed uniform liquid that is near the beginning of solid-liquid coexistence.

Before presenting evidence that the first layer has solid clusters, we first wish to demonstrate that our simulation method can reproduce the commensurate solid phase, and that this phase exhibits melting-like behavior in agreement with experiment. We then investigate the low temperature phase diagram using the Maxwell construction.

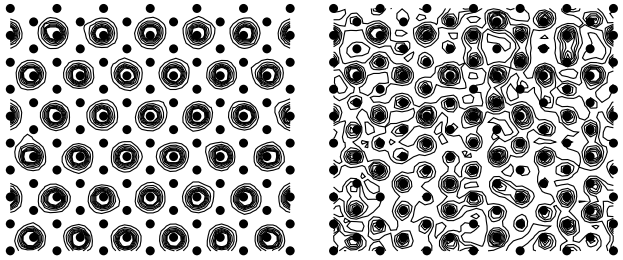

FIG. 1. Distribution plots at the commensurate density, 0.0636 atom/$\mathring{A}^2$, for T=2.99 K (left) and T=4.0 K (right). Filled circles indicate graphite adsorption sites.

Figure 1 illustrates the $\sqrt{3} \times \sqrt{3}$ commensurate solid phase and its melt using probability density contour plots. Raising the temperature from 3 K to 4 K causes melting, so that each adsorption site will, after a sufficiently long simulation run, have an equal probability of being occupied. Further evidence for solidification comes from static structure factors. Figure 2 shows our calculations at and immediately below the commensurate solid density for the (01) scattering direction. The peaks at 1.70 and 3.40 $\mathring{A}^{-1}$ are the wave vectors expected for the first two Bragg scattering peaks for the $\sqrt{3} \times \sqrt{3}$ solid.

The temperature dependence of the static structure peaks can be used to determine melting temperatures. Figure 3 shows $S(k = 1.7\mathring{A}^{-1})/N$ for several densities. Melting is signaled by a drop in the average peak height and large statistical fluctuations in peak values. This is first observed at 2 K, 2.5 K, 3 K, and 3.33 K for 0.0424, 0.0530, 0.0566, and 0.0636 atom/$\mathring{A}^{-2}$, respectively. This density dependence of melting is in agreement with the experimental phase diagram, although our melting temperatures are somewhat higher than the experimental values. Heat capacity measurements indicate the commensurate solid melts at 3 K, and the low density (≤ 0.045 atom/$\mathring{A}^{-2}$) melting peaks are at about 1.5 K.

We have also calculated the temperature dependence of the energy per particle for several densities. These possess inflection points that produce heat capacity peaks

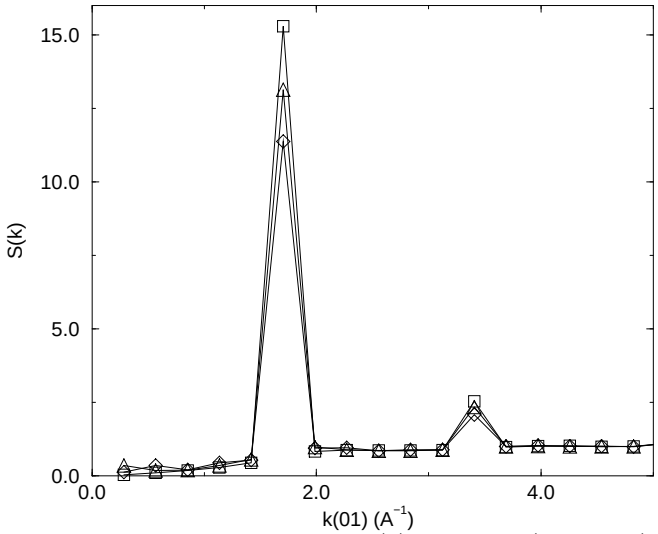

FIG. 2. Static structure factor S(k) for 0.0530 (diamonds), 0.0566 (triangles) and 0.0636 atom/$\mathring{A}^2$ (squares) at 2.0 K. The particle numbers are are 30, 32, and 36, respectively.

when the values are differentiated, signaling melting. Two sample calculations of the specific heat are shown in Fig. 4. At the commensurate density, we observe that melting occurs at about 3.5 K, somewhat above the experimental value but consistent with the static structure calculations. As the density decreases, the melting temperature and peak height also decrease. At 0.0353 atom/$\mathring{A}^2$, the melting temperature is about 1.5 K, and the peak is much smaller and more rounded.

The binding energy E_B of a single particle on the substrate may be easily calculated. We find $E_B = -145.48 \pm 0.21$, which is comparable to, but slightly lower than, the estimated values of -141.75 ± 1.50 K from scattering [21] and -142.33 ± 1.97 K from thermodynamic analysis [22]. Subtracting E_B from the energy per particle at ρ_c, we find the solid binding energy is -2.21 ± 0.20 K. This is lower than either the energy per particle of the 2D liquid or solid determined in Ref. [14].

Having demonstrated that our simulation method can reproduce known features of the monolayer, we now turn to the low density phase. This region is investigated by applying the Maxwell common tangent construction to the low temperature values of the total energy to identify unstable regions at effectively zero temperature. The application of this method to a system with a constant volume and varying particle number is described in Refs. [19]. The free energy at nonzero temperatures is not directly accessible from PIMC calculations, but we may determine effectively zero-temperature energy values by a limiting process [19]. The total free energy and total energy are the same at zero temperatures.

The coexistence region between two stable phases is characterized by an unphysical upward curvature of the total (free) energy. In the thermodynamic limit, the energy values lie on a coexistence line. Such an unstable

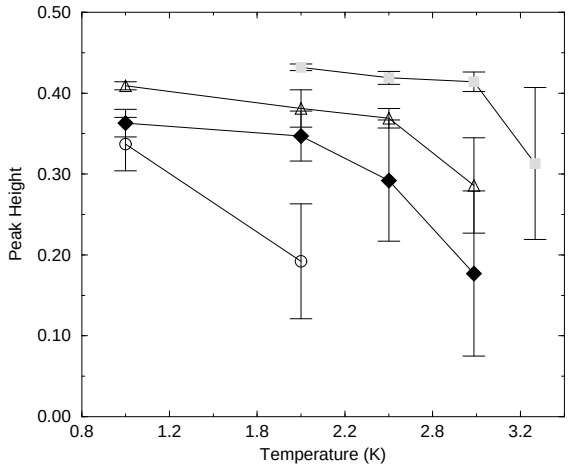

FIG. 3. Temperature dependence of the peak height of the static structure factor. The coverages are 0.0424 (circles), 0.0530 (filled diamonds), 0.0566 (triangles), and 0.0636 atom/$\mathring{A}^2$ (filled squares).

region may be identified between zero coverage and ρ_c in the total energy values shown in Fig. 5. We have verified that all these energy values have approached the zero-temperature limit within error bars. All intermediate energy values are above the coexistence line. In the unstable region, the system can phase separate into a zero density vapor and a commensurates solid cluster. The energy increase results from the finite cost of creating the phase boundary.

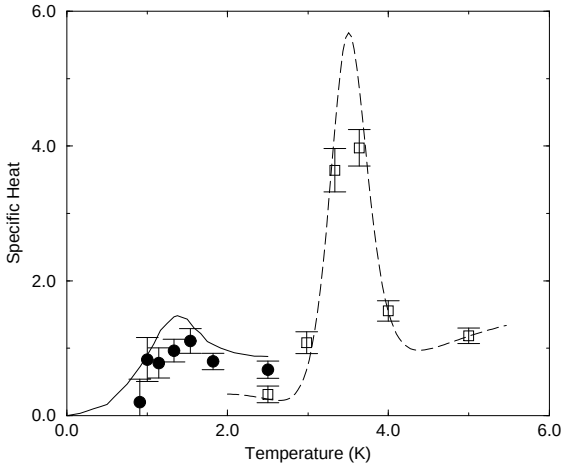

FIG. 4. The heat capacity at 0.0353 (filled circles) and 0.0636 atom/$\mathring{A}^2$ (squares). The dashed line is a guide to the eye. The solid line is the measured specific heat at 0.0367 taken from Ref. [9]

Contour plots of the probability density, shown in Fig. 6, provide direct evidence that both solid-vapor coexistence and solid phases with vacancies occur. At the lower temperature (left-hand side of Fig. 6), the vacancies have coalesced. Note that there is only one bubble in the left-hand side of Fig. 6 because of periodic boundary conditions. The holes move very slowly at this temperature, producing long equilibration times for condensation. We thus calculated the energy for this system with the vacancies initially separated and then initially condensed. The energy for condensed vacancies was lower. At higher temperatures, the vacancies acquire enough kinetic energy to leave the phase separated state and diffuse into the solid. As a result, vacancies can become isolated. This is illustrated at 2.5 K in the right-hand plot of Fig. 6. A series of probability distribution plots reveals that these vacancies move in the simulation, so the equilibration problem encountered at 1.0 K is not present at this temperature. We note that in our simulation there is still evidence of phase separation in contour plots at 2.0 K for the density shown in Fig. 6, while experimental results seem to indicate a transition at 1.5 K. We have plotted probability contours for densities as low as 0.0207 atom/$\mathring{A}^2$ and observe solid clusters at all densities.

We have also attempted to place a vacancy in a solid cluster surrounded by vapor at 0.0424 atom/$\mathring{A}^2$ and 1.0 K. The vacancy was spontaneously expelled from the cluster during thermalization, from which we conclude that the solid clusters cannot also contain isolated vacancies when in equilibrium with the low density vapor.

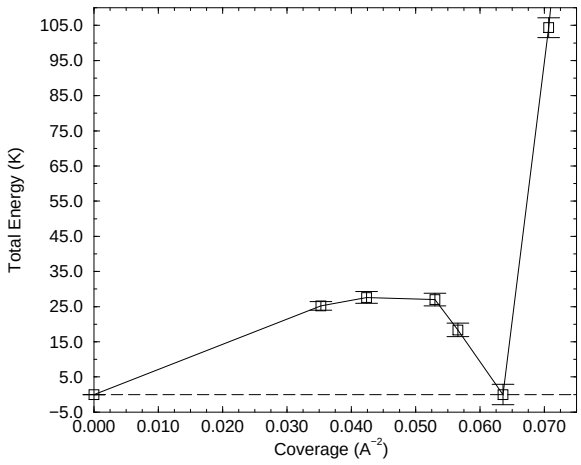

FIG. 5. Total energy versus coverage. For clarity, the energy values have been shifted by the line Ne_0, where N is the number of particles, and $e_0 = -147.78 \pm 0.08$, the minimum energy per particle. e_0 occurs at the commensurate density. The dashed line is the gas-solid coexistence line.

Finally, we wish to discuss the arguments of Greywall and Busch (GB) against solid clusters and in favor of the superfluid phase. Their primary objection to solid-vapor coexistence is that this should be signaled by linear heat

capacity isotherms for the entire region from zero coverage up to the commensurate density. Their published data shows that for temperatures from 0.2 K to 0.5 K, the isotherms are linear only between 0.025 and 0.060 atom/$\mathring{A}^2$. At 0.1 K, the upper endpoint is about 0.055 atom/$\mathring{A}^2$. As a possible explanation, we suggest that the departure from linearity below 0.025 atom/$\mathring{A}^2$ is caused by the presence of multiple finite-sized clusters. At low densities, solid clusters nucleate around surface defects. Initially, there are many small metastable clusters with large perimeter-to-area ratios. Increasing the density increases the size of the clusters until the surface is covered by a few large solid clusters with negligible boundary effects. Thus, the heat capacity exhibits linear behavior only after the solid clusters are sufficiently large so that the perimeter-to-area ratio is small. This presumably occurs for coverages above 0.025 atom/$\mathring{A}^2$. GB have used a similar explanation in their arguments for solid-liquid and liquid-gas coexistence in regions that do not have linear isotherms.

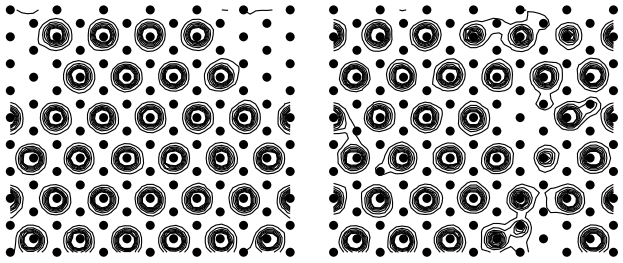

FIG. 6. Probability distributions for 0.0566 atom/$\mathring{A}^2$ at T=1.0 (left) and 2.5 K (right). The filled circles give the locations of graphite potential minima.

GB are lead to identify coverages near 0.04 atom/$\mathring{A}^2$ as liquid based partly on simulation results for 2D helium on a flat substrate, which were the most relevant calculations then available. As GB note, the large peak associated with the melting of the uniform commensurate solid phase first emerges at 0.04 atom/$\mathring{A}^2$. 2D helium is a liquid near this density [23], suggesting that first layer coverages below 0.04 may be liquid. Unlike the purely 2D simulations, our calculations take the role of substrate effects into account. As we have shown, surface corrugations push the density of the energy minimum up from about 0.04 on a flat substrate to 0.0636 atom/$\mathring{A}^2$ and produce solidification. GB also show that their heat capacity results are in general agreement with a PIMC calculation for 2D superfluid helium [24], suggesting that there might be a superfluid transition in the first layer. We have shown in Fig. 4 that the rounded heat capacities seen for low first layer densities are produced by the melting of a solid cluster and are not associated with a superfluid transition.

This work was supported in part by the National Aeronautics and Space Administration under grant number NAG3-1841. Some of the calculations for this work were performed using the facilities of the Supercomputer Computations Research Institute at Florida State University.

[1] J. G. Dash, *Films on Solid Surfaces* (Academic, New York, 1975).
[2] M. Schick, in *Phase Transitions in Surface Films*, edited by J. G. Dash and J. Ruvalds (Plenum, New York, 1980).
[3] L. W. Bruch, M. W. Cole, and E. Zaremba, *Physical Adsorption: Forces and Phenomena* (Oxford, New York, 1997).
[4] M. Bretz *et al.*, Phys. Rev. A **8**, 1589 (1973).
[5] D. S. Greywall, Phys. Rev. B **47**, 309 (1993).
[6] M. Nielsen, J. P. McTague, and L. Passell, in *Phase Transitions in Surface Films*, edited by J. G. Dash and J. Ruvalds (Plenum, New York, 1980).
[7] F. F. Abraham and J. Q. Broughton, Phys. Rev. Lett. **59**, 64 (1987).
[8] R. E. Ecke, Q.-S. Shu, T. S. Sullivan, and O. E. Vilches, Phys. Rev. B **31**, 448 (1985).
[9] D. S. Greywall and P. A. Busch, Phys. Rev. Lett. **67**, 3535 (1991).
[10] J. M. Mochel and M.-T. Chen, Physica B **197**, 278 (1994); M. Boninsegni and M. W. Cole, J. Low Temp. Phys. **113**, 393 (1998); J. Nyéki, R. Ray, B. Cowan, and J. Saunders, Phys. Rev. Lett. **81**, 152 (1998).
[11] M. Bretz, Phys. Rev. Lett. **31**, 1447 (1973).
[12] A. N. Berker, S. Ostlund, and F. A. Putnam, Phys. Rev. B **17**, 3650 (1978).
[13] M. Schick, J. S. Walker, and M. Wortis, Phys. Rev. B **16**, 2205 (1977).
[14] J. M. Gottlieb and L. W. Bruch, Phys. Rev. B **48**, 3943 (1993).
[15] P. A. Crowell and J. D. Reppy, Phys. Rev. B **53**, 2701 (1996).
[16] R. A. Aziz *et al.*, Mol. Phys. **77**, 321 (1992).
[17] W. E. Carlos and M. W. Cole, Surf. Sci. **91**, 339 (1980).
[18] D. M. Ceperley, Rev. Mod. Phys. **67**, 279 (1995).
[19] M. Pierce and E. Manousakis, Phys. Rev. Lett. **81**, 156 (1998); M. Pierce and E. Manousakis, accepted for publication in Phys. Rev. **B**.
[20] P. A. Whitlock, G. V. Chester, and B. Krishnamachari, Phys. Rev. B **58**, 8704 (1998).
[21] W. E. Carlos and M. W. Cole, Phys. Rev. B **21**, 3713 (1980).
[22] R. L. Elgin and L. Goodstein, Phys. Rev. A **9**, 2657 (1974).
[23] P. A. Whitlock, G. V. Chester, and M. H. Kalos, Phys. Rev. B **38**, 2418 (1988).
[24] D. M. Ceperley and E. L. Pollock, Phys. Rev. B **39**, 2084 (1989).